### Microscopic Detection and Control of In-plane Surface Mechanical Properties on Anthracene Crystal by Using a Femtosecond Laser and an Atomic Force Microscope

Yuhau Ye<sup>1</sup>, Yuka Tsuri\*1,2, and Yoichiroh Hosokawa\*1,2

<sup>1</sup>Division of Materials Science, Nara Institute of Science and Technology, Japan <sup>2</sup>Medilux Research Center, Nara Institute of Science and Technology, Japan \*Corresponding authors' e-mail: tsuri.yuka@ms.naist.jp, hosokawa@ms.naist.jp

An infrared femtosecond laser pulse was focused on an anthracene crystal surface to generate a stress wave, and its propagation on the crystal was detected by an atomic force microscope (AFM). Additionally, femtosecond laser pulses were employed to modify the crystal surface. The wave propagation velocity was estimated from the delay time between the pulse irradiation time and the first response of cantilever, which depended on the distance between the laser focal point and the contact point of cantilever. Utilizing partial least squares discriminant analysis (PLS-da) of the waveform of the cantilever response, we found that propagation behavior of the wave was modified between unmodified and laser-modified surfaces. These results suggested that the detected wave propagation was dominated by the surface acoustic wave (Rayleigh wave). The propagation velocity of the surface waves provides the Young's modulus of the crystal, which was estimated to be 655 MPa. This is much smaller than that (5 GPa) estimated by the conventional AFM indentation test. These respective values are considered to predominantly reflect the in-plane and out-of-plane mechanical properties of the anthracene crystal surface. We show a novel method for characterizing in-plane mechanical properties of organic crystal surfaces.

DOI: 10.2961/ilmn.2025.03.2016

**Keywords:** femtosecond laser, atomic force microscopy, machine learning, Young's modulus, crystal surface, organic compound

#### 1. Introduction

The mechanical properties of organic crystals are drastically modified by nano- and micro-structures that disrupt the periodic molecular arrangement in the crystals, such as defects, cracks, and phase transitions [1–7]. In particular, the properties of crystal surfaces are strongly influenced by the defects and cracks localized on the surfaces. In addition, the surface properties are further modulated when the surfaces are immersed in solvents or exposed to water moisture. Detection and control of such nano- and micro-scale surface mechanical properties is an essential requirement for device applications [8–11].

Atomic force microscopy (AFM) has been widely utilized to determine local mechanical properties of material surfaces [12]. The AFM utilizes to estimate the surface elasticity in the out-of-plane direction, but it is difficult to detect the properties in the in-plane direction, which strongly reflect the properties localized on the crystal surface. For this detection of properties in the in-plane direction, we have applied a femtosecond laser as an impulse generator [13–23]. When an intense femtosecond pulse is focused on the crystal surface through an objective lens, an impulse is generated at the laser focal point, and it propagates on the surface as a shock wave and a stress wave [24–28].

We have developed a method to prove the vibrational response due to the impulse, which is detected by the AFM cantilever contacting near the laser focal point [29–32] and

named this method pulsed laser activated impulse response encoder (PLAIRE) [33].

Previously, we applied the PLAIRE to surface stiffness evaluation of zebrafish embryos [34]. The embryo consists of an inner yolk and an outer surface cell layer. In the AFM indentation test, which is commonly used to measure Young's modulus, an average of the properties of the components of the embryo is taken. In contrast, in the PLAIRE method, femtosecond laser impulses excite vibrations directly in the surface layer, allowing the surface stiffness to be distinguished from the bulk.

In the present study, we demonstrated the potential of the PLAIRE method to measure surface stiffness using anthracene crystal, which is a representative organic crystal. In addition, the femtosecond laser was used to produce a groove on the crystal surface. We expected the groove would modify the propagation of the surface acoustic wave (Rayleigh wave) on the crystal. We evaluated the modification of the wave propagation by partial least squares discriminant analysis (PLS-da) combined with a support vector machine (SVM). The result indicated a possibility that the propagation was visualized by the machine learning process. Based on these results, we showed that the PLAIRE method specifically detected mechanical properties on the in-plane surface of the organic crystal.

#### 2. Methods

#### 2.1 Sample preparation

As the sample, we prepared anthracene crystals by the following process. Anthracene powder (NACALAI TESQUE, INC., Lot No. M1T4947) was dissolved into cyclohexane (Wako, Lot No. TPH2912) in a covered 30 mL glass bottle at a concentration of 20 mM. The solution was heated to 60°C in an incubator (Tokyo Rikakikai, LTE-510) for 6 h to completely dissolve the anthracene.

After that, the solution was cooled to 25°C and disturbed with a pipette tip to induce crystallization. After 24 h at 15°C in the incubator, a few single anthracene crystals were precipitated at the bottom of the bottle. The upper solution was removed using a pipette, and then the uncovered glass bottle was returned to the incubator at 15°C until the solvent completely evaporated.

#### 2.2 Optical setup for PLAIRE

The experimental setup for measuring vibrational responses propagating in anthracene crystal is given in Fig. 1. A single laser pulse from a regeneratively amplified Ti:sapphire femtosecond laser (Spectra-Physics, Solstice-Ace; wavelength, 800 nm; pulse duration, 100 fs; repetition rate, 32 Hz) was introduced into an inverted microscope (Olympus, IX71) and focused on the upper surface of an anthracene crystal (001-plane) through a 20× objective lens (Olympus, UMPlanFl; N.A. 0.46). The single pulse was extracted using a mechanical shutter with a 33 ms gate time. The pulse energy was tuned at 1  $\mu J/pulse$  by polarizers and neutral density filters.

The vibrational response induced on the anthracene crystal was detected by an AFM (JPK Instrument, Nanowizard 4) through an AFM cantilever (MikroMasch, XSC11-A; shape, rotated pyramidal; spring constant, 0.2 N/m) that contacted on the upper crystal surface at a certain distance to the laser focal point. The temporal movement of the cantilever associated with the crystal vibration was recorded by an oscilloscope (Tektronix, DPO 4104), which acquired data with a temporal resolution of 0.2 ns per point.

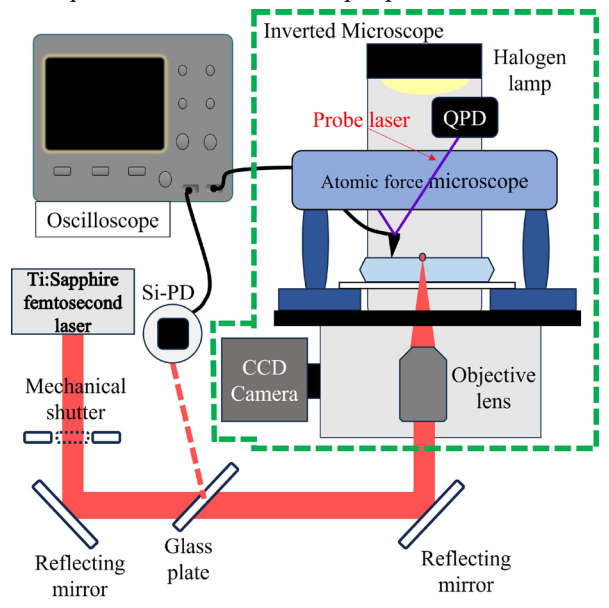


Fig. 1 Schematic illustration of the experimental setup.

The stage for the sample was motorized, and its translational and axial motions were computer controlled. We examined the vibration behavior as a function of the distance between the cantilever and the laser focal point. The femtosecond laser was also used to form a groove on the crystal surface. The laser pulses (pulse energy, 1  $\mu$ J/pulse; repetition rate, 1 kHz) were scanned on the surface with scanning speed of 35  $\mu$ m/s.

#### 2.3 Classification of vibrations by machine learning

To identify the type of vibration, we compared the vibrational response of crystals with different surface conditions. One was a crystal whose surface was processed with a femtosecond laser (with the groove), and the other was the intact crystal (without the groove). We evaluated the vibrational responses by using PLS-da and the SVM[35–37]. PLS-da was employed to identify subtle differences by reducing the dimensionality of the dataset. The top ten PLS-da components (components 1 to 10) with the highest contributions were extracted from the vibration data.

To evaluate the classification performance, we scored component combinations in vibration responses before and after the laser processing, compared all possible pairs of PLS-da components (from 1 to 10), and analyzed them using SVM classifiers which is a type of supervised machine learning. Specifically, SVM was trained in a two-dimensional feature space defined by a component pair, and the classification accuracy was used to identify the pairs providing the best class separation.

#### 2.4 AFM Indentation test

The indentation test used the AFM equipped with a conical type of cantilever (NANOSENSORS, T7L cantilever; spring constant, 440 N/m). In the force curve measurements, the indentation of the crystal surface due to the contact of the AFM cantilever was detected as a function of the force applied to the cantilever. The force-indentation curve was fitted by an equation based on Hertz contact theory to estimate the Young's modulus.

#### 3. Results and discussion

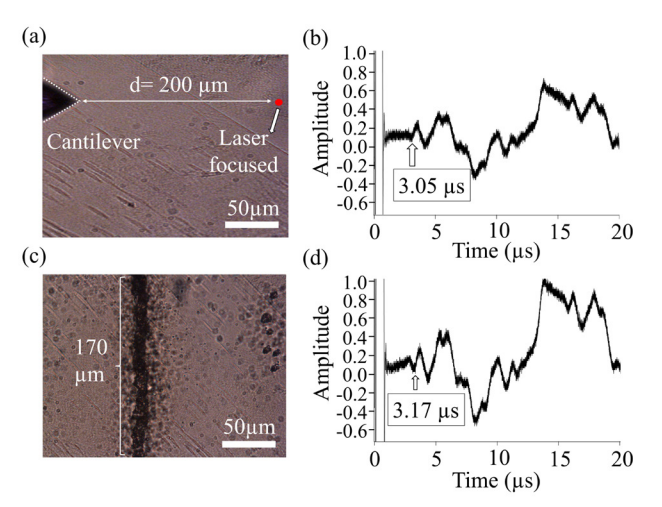
## 3.1 Identification of the waves detectable by the PLAIRE method

Fig. 2(a) shows a microphotograph of the crystal surface including the relationship between the cantilever and the laser focus. Fig. 2(b) shows the vibrational response of the cantilever at 200  $\mu$ m between the contact point of the cantilever and the laser focal point. A sharp and intense vibration appeared immediately after the laser irradiation (< 0.5  $\mu$ s) in the waveform. This vibration is an artifact due to the scattering of the femtosecond laser beam to the photodiode in the AFM. After the fast vibration, we observed a subsequent vibration.

The time of first propagation wave after the femtosecond laser induced scattering in Fig. 2(b) was identified at the time when the normalized amplitude first exceeded the noise level in the range of 0.0 to 0.2. This reproducibility was checked by repeating the measurements at the same position and estimating under different conditions, such as when using different crystals or measuring different locations on the same crystal. Fig. 2(c) is the microphotograph of a crystal

with a groove with length of 170  $\mu m$ . The distance from the cantilever to the center of the groove was set to be 100  $\mu m$  which was same as the distance from the groove center to the laser focal spot. Fig. 2(d) shows the vibrational response for the crystal with the groove.

The arrival time of the first wave was  $3.17~\mu s$ . In Fig. 2(b) and 2(d), a time delay of  $0.12~\mu s$  in the first arrival was observed when the crystal surface was modified by the laser irradiation, although the distance between the cantilever and the laser focus remained constant.



**Fig. 2** (a) Microphotograph of the crystal surface and the top of the AFM cantilever. The laser focal point is indicated by a red circle. (b) The vibrational responses induced by the laser irradiation on the crystal surface. The arrow indicates the arrival time of the first wave. (c) Microphotograph of crystal surface with a 170  $\mu$ m long groove produced by the femtosecond laser processing. (d) The vibrational responses of the crystal surface with the 170  $\mu$ m groove. The arrow indicates the arrival time of the first wave.

This result indicated that the groove prevented the wave propagation, suggesting that the waves reflected the crystal-line surface condition. As the wave propagated through the crystal, there are two possibilities: a Rayleigh wave propagating along the crystal surface and a pressure wave propagating within the crystal. To consider these two possibilities, we assessed the propagation velocity from the relationship between the arrival time of the vibration and the distance between the laser focal point and the AFM contact point. Based on eleven experimental measurements varying the distance from 100 to 400  $\mu m$  for six crystals, the wave propagation velocity was determined to be 403 m/s.

This velocity is significantly slower than the pressure wave velocity (~1700 m/s) propagating inside the bulk crystal [38]. It is known that the surface acoustic wave propagates more slowly than the pressure wave [39]. The modification of wave propagation by creating the surface groove indicates that the PLIARE is sensitive to the crystal surface. These results suggest that the primary component of the vibrational response detected by the PLIARE is the surface acoustic wave that propagates on the crystal.

# 3.2 Partial least squares discriminant analysis (PLS-da) combined with the support vector machine (SVM)

The vibrational response should contain structural information about the crystal surface. On the other hand, the

waveform is too complex to be understood by simple physics. Therefore, we applied a data analysis based on machine learning. The dataset comprising 54 vibrational responses (The 29 red dots and 25 blue dots correspond to the crystal with and without the groove, respectively) collected from four different crystals were classified by PLS-da. We extracted the highest contributing components from first to tenth by PLS-da analysis and scored based on the amount of the analyzed components contained in each wave.

The combination of the scores between the first and seventh components (components 1 and 7) was found to provide the clearest separation of the samples as shown in Fig. 3(a). The boundary of the red and blue areas indicates the score combination for the crystal with and without the groove that was determined by the SVM. When components 1 and 7 were used as input for the SVM classification, the accuracy approached 94%. This result indicated that the vibrational response detects the difference in wave propagation on the crystal surfaces with and without the groove.

To identify which features contributed to this high classification performance, the PLS-da results were further analyzed in terms of loading values, where larger absolute values correspond to greater importance for classification. As shown in Fig. 3(b), the loading values of components 1 and 7 reach maximum before 12 μs and decrease at the late stage. Since larger absolute value in the loading includes the more significant information for classification, major contribution of components 1 and 7 are before 12 μs. This result suggests that the essential information related to surface modification is primarily contained in the early stage of the vibration before 12 μs.

This result suggested the potential of the PLS-da analysis for analyzing wave propagation on the crystal surface.

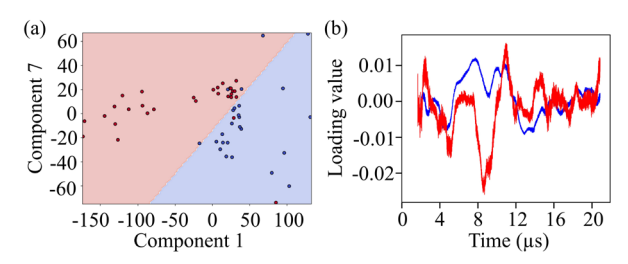


**Fig. 3** (a) Classification of the vibrational response on the crystal surface with and without the groove in 54 experimental runs. The PLS-da scores of components 1 and 7 were plotted as horizontal and vertical axes. (b) The loading values of component 1 (blue line) and component 7 (red line) vs. time.

# 3.3. Comparing Young's modulus estimated by the PLAIRE method and the indentation test

From the above results, we considered that the vibrational response was due to a surface acoustic wave, also known as Rayleigh wave. The propagation velocity of the Rayleigh wave ( $V_R$ ) is related to Young's modulus (E) of the crystal as follows [40]:

$$V_R = \sqrt{\frac{0.87E}{2\rho(1+v)}},$$
 (1)

where  $\rho$  is the anthracene density with given values of 1280 kg/m<sup>3</sup> and v is Poisson's ratio (0.32 for anthracene crystal) [38]. The average of E obtained from the averaged  $V_R$  (403 m/s) is 655 MPa.

Alternatively, the Young's modulus of the crystals was also estimated by a conventional indentation test using AFM. In the analysis, we applied the Hertz model to estimate the Young's modulus of the crystals. The relationship between the force and the indentation depth of the surface is shown in Fig. 4(a). Young's modulus of the crystal was analyzed by fitting the force-indentation curve predicted by Hertz-Sneddon model based on Hertz contact theory[41,42].

The maximum indentation depth for the fitting was set to be molecular scale (30 nm); however, the fitting accuracy was unsatisfactory even for this very small indentation. The Young's modulus was about 5 GPa in 40 experimental measurements (Fig. 4(b)), which was about eight times larger than the modulus estimated from the Rayleigh wave by the PLAIRE method (655 MPa). In the previous work [38], the Young's modulus of anthracene crystal was estimated by single crystal X-ray diffraction with computation, and the value has been estimated to be about 10 GPa, which is closer to the Young's modulus by the AFM indentation test rather than that estimated by the PLAIRE.

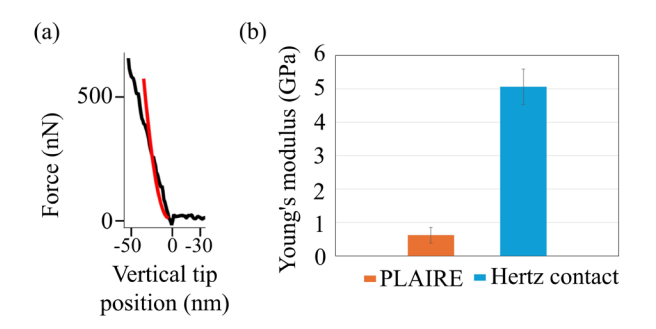


**Fig. 4** (a) Representation of the force-indentation curve measured by the conventional AFM indentation test. The red line is the Hertz-Sneddon model fit curve. (b) Distribution of Young's modulus estimated by the PLAIRE (left) and the AFM indentation test (right).

Here, we discuss the origin of this difference of measured Young's modulus. We consider this difference in the deformation direction relative to the crystal surface. The AFM indentation test detects Young's modulus inside the crystal in the out-of-plane direction from the surface to the bulk, as shown in Fig. 5(a). In contrast, the present method presumably detects the Rayleigh wave which propagates on the surface layer (Fig. 5(b)), i.e. the estimated Young's modulus strongly reflects the condition of the surface layer in the inplane direction. The crystal surface generally exhibits higher surface energy and weaker intermolecular bonding than the bulk region, which makes it more susceptible to deformation.

One possible reason for the marked disparity between the two Young's moduli is that a less stable molecular arrangement on the crystal surface results in a lower Young's modulus[43,44]. The detailed mechanism should be clarified through experiments with varying surface conditions and analysis based on machine learning.

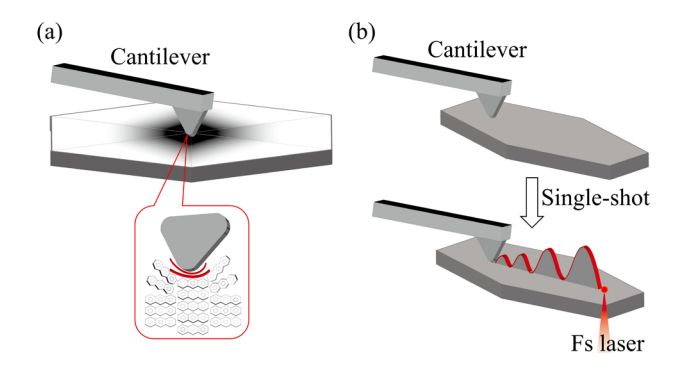


**Fig. 5** Force in the detection of the AFM cantilever. (a) The tip of the AFM cantilever pushed onto the crystal surface senses the stiffness from the molecular arrangements in the out-of-plane direction. (b) The tip detects Rayleigh wave vibrations propagating on the crystal surface.

#### 4. Conclusions

We successfully demonstrated potential of the PLAIRE method for detecting the mechanical properties of organic crystal surfaces. We identified the origin of the vibration detected by the PLAIRE as the Rayleigh wave on the crystal surface through evaluations by velocities of waves, crystal surface modifications, and machine learning classification. Furthermore, the machine learning analysis indicated that the detected vibration is very sensitive for the surface condition

Based on these results, we estimated Young's modulus on the in-plane crystal surface was 655 MPa, which was extremely smaller than that (5 GPa) on the out-of-plane crystal surface estimated by the conventional AFM indentation test. The PLAIRE method provides valuable insights into future applications of organic crystals in device design and crystallography.

#### Acknowledgments

This work was supported by Grant-in-Aid for Early-Career Scientists (No. 23K13673 for YT).

#### References

- [1] A.R. Galamay, D. V. Sydor, and F. Meng: Minerals, 10, (2020) 1.
- [2] M. Li, C. Zhang, M. Li, F. Liu, L. Zhou, Z. Gao, J. Sun, D. Han, and J. Gong: J. Chem. Eng., 429, (2022) 132450.
- [3] J. Li, C.J. Tilbury, S.H. Kim, and M.F. Doherty: Prog Mater Sci, 82, (2016) 1.
- [4] D.P. Woodruff: Philos. Transact. A Math. Phys. Eng. Sci., 373, (2015) 20140230.
- [5] V. Ehrlacher, C. Ortner, and A. V. Shapeev: Arch Ration Mech Anal, 222, (2016) 1217.
- [6] Y. Zheng, T.J. Slade, L. Hu, X.Y. Tan, Y. Luo, Z.-Z. Luo, J. Xu, Q. Yan, and M.G. Kanatzidis: Chem Soc Rev, 50, (2021) 9022.
- [7] G. Staikov and W.J. Lorenz: Can J Chem, 75, (1997) 1624.
- [8] L. Addadi, L. Kronik, L. Leiserowitz, D. Oron, and S. Weiner: Adv. Mater., 36, (2024) 2408060.
- [9] M.D. Ward: Curr Opin Colloid Interface Sci, 2, (1997) 51.

- [10] W. Littke, M. Haber, and H.-J. Gu"ntherodt: J Cryst Growth, 122, (1992) 80.
- [11] Y. Tsuri, M. Maruyama, H.Y. Yoshikawa, S. Okada, H. Adachi, K. Takano, K. Tsukamoto, M. Imanishi, M. Yoshimura, and Y. Mori: J Cryst Growth, 532, (2020) 125430.
- [12] Q.S. Li, G.Y.H. Lee, C.N. Ong, and C.T. Lim: Biochem Biophys Res Commun, 374, (2008) 609.
- [13] Y. Hosokawa, M. Hagiyama, T. Iino, Y. Murakami, and A. Ito: PNAS, 108, (2011) 1777.
- [14] R. Yasukuni, J.A. Spitz, R. Meallet-Renault, T. Negishi, T. Tada, Y. Hosokawa, T. Asahi, C. Shukunami, Y. Hiraki, and H. Masuhara: Appl Surf Sci, 253, (2007) 6416.
- [15] L. V. Zhigilei and B.J. Garrison: J Appl Phys, 88, (2000) 1281.
- [16] K. Oikawa, S. Matsunaga, S. Mano, M. Kondo, K. Yamada, M. Hayashi, T. Kagawa, A. Kadota, W. Sakamoto, S. Higashi, M. Watanabe, T. Mitsui, A. Shigemasa, T. Iino, Y. Hosokawa, and M. Nishimura: Nat Plants, 1, (2015) 15035.
- [17] Y. Hosokawa, H. Takabayashi, S. Miura, C. Shukunami, Y. Hiraki, and H. Masuhara: Appl. Phys. A: Mater. Sci. Process., 79, (2004) 795.
- [18] A. Takita and Y. Hayasaki: Jpn J Appl Phys, 48, (2009) 09LD04.
- [19] Y. Hosokawa: Jpn J Appl Phys, 58, (2019) 110102.
- [20] A. Vogel and V. Venugopalan: Chem Rev, 103, (2003) 577.
- [21] Y. Tsuri, N. Inaoka, M. Maruyama, K. Tsukamoto, H. Adachi, H.Y. Yoshikawa, K. Takano, M. Imanishi, M. Yoshimura, and Y. Mori: J Cryst Growth, 557, (2021) 125994.
- [22] Y. Tsuri, M. Maruyama, R. Fujimoto, S. Okada, H. Adachi, H.Y. Yoshikawa, K. Takano, S. Murakami, H. Matsumura, T. Inoue, K. Tsukamoto, M. Imanishi, M. Yoshimura, and Y. Mori: Appl. Phys. Express, 12, (2019) 015507.
- [23] A. Vogel, J. Noack, G. Hüttman, and G. Paltauf: Appl. Phys. B: Lasers Opt., 81, (2005) 1015.
- [24] L. V Zhigilei, P.B.S. Kodali, and B.J. Garrison: J. Phys. Chem. B, 102, (1998) 2845.
- [25] B.J. Garrison, T.E. Itina, and L. V. Zhigilei: Phys Rev E Stat Phys Plasmas Fluids Relat Interdiscip Topics, 68, (2003) 041501.
- [26] H. Masuhara: Bull Chem Soc Jpn, 86, (2013) 755.
- [27] M.K. Bhuyan, A. Soleilhac, M. Somayaji, T.E. Itina, R. Antoine, and R. Stoian: Sci Rep, 8, (2018) 9665.
- [28] Y. Hosokawa, M. Yashiro, T. Asahi, and H. Masuhara: J Photochem Photobiol A Chem, 142, (2001) 197.
- [29] T. Iino and Y. Hosokawa: Appl. Phys. Express, 3, (2010) 107002.
- [30] T. Iino and Y. Hosokawa: J Appl Phys, 112, (2012) 066106.
- [31] M. Takenaka, T. Iino, A. Nagatani, and Y. Hosokawa: Appl. Phys. Express, 7, (2014) 087002.
- [32] T. Iino, P. Li, W. Wang, J. Deng, Y. Lu, F. Kao, and Y. Hosokawa: Appl. Phys. A: Mater. Sci. Process., 117, (2014) 389.
- [33] R. Yasukuni, R. Fukushima, T. Iino, and Y. Hosokawa: Appl. Phys. Express, 10, (2017) 117001.

- [34] R. Yasukuni, D. Minamino, T. Watanabe, S. Yamada, T. Iino, Y. Bessho, T. Matsui, and Y. Hosokawa: Appl Phys A Mater Sci Process, 124, (2018) 594.
- [35] E. Sufriadi, R. Idroes, H. Meilina, A.A. Munawar, N. Lelifajri, and G. Indrayanto: ACS Omega, 8, (2023) 12348.
- [36] M. Shih, Y. Yuan, and G. Shi: J Anal At Spectrom, 39, (2024) 1560.
- [37] G. Yang, S. Qiao, P. Chen, Y. Ding, and D. Tian: Plasma Sci. Technol., 17, (2015) 656.
- [38] T.L. Prazyan and Y.N. Zhuravlev: Int. J. Mod. Phys. C, 29, (2018) 1850024.
- [39] H. Nakaoka: AIP Adv, 14, (2024) 075004.
- [40] M. Li and Z. Feng: Rev. Sci. Instrum., 87, (2016)
- [41] I.N. Sneddon: Int J Eng Sci, 3, (1965) 47.
- [42] I.V.M. Lima, A.V.S. Silva, F.D. Sousa, W.P. Ferreira, R.S. Freire, C.L.N. de Oliveira, and J.S. de Sousa: Heliyon, 10, (2024) e30623.
- [43] R. Tran, Z. Xu, B. Radhakrishnan, D. Winston, W. Sun, K.A. Persson, and S.P. Ong: Sci Data, 3, (2016) 160080.
- [44] G. Volonakis, L. Tsetseris, and S. Logothetidis: Mater. Sci. Eng. B, 176, (2011) 484.

(Received: June 30, 2025, Accepted: November 9, 2025)